





Article

Analysis of the Effect of Soil Erosion in Abandoned Agricultural Areas: The Case of NE Area of Basilicata Region (Southern Italy)

Valentina Santarsiero ^{1,2,3}, Antonio Lanorte ^{1,*}, Gabriele Nolè ¹, Giuseppe Cillis ¹, Biagio Tucci ¹ and Beniamino Murgante ²

¹ CNR IMAA, Tito Scalo, 85050 Potenza, Italy

² School of Engineering, University of Basilicata, 85100 Potenza, Italy

³ CNR IGAG, Area Della Ricerca di Roma 1, Strada Provinciale 35d, 00185 Rome, Italy

* Correspondence: antonio.lanorte@imaa.cnr.it

Abstract: Land abandonment is among the most complex land use change processes driven by a multiplicity of anthropogenic and natural factors, such as agricultural over-exploitation, implementation of agricultural policies, socio-economic and climatic aspects. Therefore, it is necessary to deepen the effects of land abandonment based on methodologies that are as multidisciplinary as possible. Environmental and social problems related to abandonment include soil erosion and environmental degradation. Approaches combining GIS (Geographic Information System), remote sensing, and image analysis techniques allow for assessments and predictions based on integrating theoretical models with advanced geospatial and geostatistical models. One of the most widely used models for soil erosion estimation is the Revised Universal Soil Loss Equation (RUSLE). The present work developed a model using remote sensing and GIS tools to investigate some factors of the RUSLE equation to evaluate the adverse effects of soil erosion in areas covered by arable crops and subsequently abandoned. To identify potentially degraded areas, two factors of the RUSLE were related: the C Factor describing the vegetation cover of the soil and the A Factor representing the amount of potential soil erosion. Through statistical correlation analysis with the RUSLE factors, based on the deviations from the average erosion values and mapping of the areas of vegetation degradation relating to arable land, the areas identified and mapped are susceptible to soil degradation.

Keywords: land abandonment; soil erosion; remote sensing; GIS



Citation: Santarsiero, V.; Lanorte, A.; Nolè, G.; Cillis, G.; Tucci, B.; Murgante, B. Analysis of the Effect of Soil Erosion in Abandoned Agricultural Areas: The Case of NE Area of Basilicata Region (Southern Italy). *Land* **2023**, *12*, 645. <https://doi.org/10.3390/land12030645>

Academic Editors: Ilan Stavi and Manuel Pulido Fernández

Received: 8 February 2023

Revised: 1 March 2023

Accepted: 5 March 2023

Published: 9 March 2023



Copyright: © 2023 by the authors. Licensee MDPI, Basel, Switzerland. This article is an open access article distributed under the terms and conditions of the Creative Commons Attribution (CC BY) license (<https://creativecommons.org/licenses/by/4.0/>).

1. Introduction

Land use changes (LUC) since the 1950s represented rural areas' primary source of transformation. Land abandonment is among the most impacting land use changes in landscape and environment [1–6]. Despite the increasing demand for areas with agricultural purposes, agricultural abandonment processes show a growing trend starting from the post-World War II period, mainly caused by physical, environmental, social, and economic factors linked, for example, to agricultural overexploitation preceding the stage of abandonment [2]. In other words, land abandonment can be defined simply as the cessation of agricultural activities and management for more than five years [7] or those processes involving land recently used for agricultural purposes but currently not subject to any cultivation practice (agricultural cultivation and pasture) [8,9]. The drivers, such as soil quality, ecological vulnerability, and unfavorable pedological features, can be natural. They are also human-driven because they are linked to socioeconomic factors, demographic structure, and institutional frameworks [10–14]. Explanations of abandonment are multidimensional, and there is no clear division between drivers, as abandonment depends on the combination and iteration between the drivers mentioned above. Many authors have studied agricultural abandonment in Europe. They have demonstrated that in the

Mediterranean Basin, this process occurs mainly in less productive areas, in mountainous, marginal, and hardly accessible zones, and areas characterized by soil erosion and/or climatic conditions unsuitable for agriculture [14–16]. The causes and magnitude of the abandonment of agricultural areas vary from region to region; for example, in southern Italy's inland and marginal areas between the 1970s and 1980s, there was a constant agricultural abandonment [15,17–19]. National and European agricultural policies potentially play a decisive role in the abandonment processes [10]. Indeed, some areas in Southern Italy in the 1950s were converted into cereal crops, favored by the Agrarian Reform policies. This increased agricultural mechanization in the utilized agricultural area (UAA), even in zones considered unsuitable for arable cultivation [15,20]. In subsequent decades, as a result of changes in socio-economic conditions, crises in the agricultural sector making cereal farming economically unfavorable in many areas, and various land reforms promoted by the Common Agricultural Policy (especially the “set-aside” scheme [21,22]), there was a gradual abandonment of arable land [23]. These phenomena modeled different landscapes of climatic conditions, age of abandonment, management regime before and after the abandonment, and disturbance type. Land abandonment has social and economic effects and impacts on environmental safety, the biodiversity of agricultural areas, and landscape configuration. Agricultural abandonment can have beneficial and detrimental effects, although the consequences differ depending on location and scale [24]. The link between abandonment, soil erosion, and soil degradation requires in-depth methodological and technical investigations, as factors, dynamics, and possible correlations are very varied and often discordant. Excessive land use and abandonment may be closely linked in some territorial contexts. Some areas could be abandoned precisely because of problems resulting from agricultural overexploitation that occurred in the past. The abandonment of agricultural regions contributes, among the negative impacts, to soil erosion and land degradation [23,25]. Land degradation includes all the processes of alteration of soil conditions. It is a complex issue due to various phenomena such as aridity, soil morphology and orography, vegetation cover, and anthropic and climatic factors [26]. Among the land degradation processes, erosion is among the most impacting. Erosion is mainly due to the intensity of rainfall; when short and intense rains occur on land with no or little vegetation cover, the surface runoff removes the surface layer richest in organic matter from the soil. Among the factors predisposing to erosion, the orientation of slopes represents a factor of vulnerability in areas also subjected to water stress. Steep slopes reduce the absorption capacity and contribute to surface runoff. For example, southern slopes, exposed to more significant solar radiation with low humidity levels, present microclimatic conditions adverse to the regeneration of stable vegetation favoring the triggering of erosion processes [20,27].

Land degradation and desertification are complex processes caused by anthropic activities and soil and climatic characteristics. Spatial analysis, statistical techniques, and remote sensing have been used to identify significant degradation trends due to agricultural abandonment in the area. The combined use of satellite data and spatial analyses allows the production of data for the estimation and monitoring of land degradation and soil erosion and the mapping and monitoring of areas subject to degradation. These are mainly based on vegetation spectral indices obtained by combining the different spectral bands of Sentinel data, which emphasize and detect any changes in the vegetation status. Integrating the RUSLE soil erosion model with remote sensing models is an effective and extensively used tool in the literature [28–32], useful for mapping and quantifying soil erosion areas and rates for developing better land conservation and monitoring maps. Direct field measurements are very expensive as they require more human and technological resources [33,34] and cannot cover the whole catchment area but are limited to specific sites [33]. Empirical models, on the other hand, such as RUSLE, in a GIS environment, thanks also to the ever-increasing availability of satellite images with a high spatial resolution (for example, the data of the Sentinel constellation), can facilitate the quantitative monitoring of the rate of soil loss in large areas [35,36].

According to the data reported by Italian agricultural censuses, Basilicata is among the Italian regions with extensive arable land. In line with the national trend, a constant decrease in agricultural areas, especially arable land, has been shown [37]. Basilicata is mainly affected by the risk of land degradation; among the different degradation processes, the process of soil erosion is dominant, sometimes taking the form of typical morphological configurations (gullies and badlands). Assessing land degradation at the regional scale is of fundamental importance to characterizing land surface, its variations over time, and identifying areas needing urgent actions [38,39].

The multidisciplinary approach, such as the combination of the LULCC (Land Use Land Cover Changes) diachronic analyses associated with erosion models and land degradation estimations, represents a fundamental tool for formulating adequate land-use planning and limiting human impacts on the environment [40]. Many studies in the literature focused on land degradation assessment by applying different research methods, most of which are based on the application of spatial analysis through GIS, remote sensing, and direct soil measurements (sampling and laboratory surveys [41–44]). Remote sensing techniques are more flexible than field analysis methods because they allow for the observation of large areas using a range of spectral indices useful for characterizing those environmental phenomena that contribute to LULCC [45–48]. Remote-sensing data are of great help in supporting local government bodies in monitoring degradation phenomena [49]. The fundamental information to analyze concerns vegetation cover, rainfall, surface runoff, and soil erosion. Furthermore, empirical models can be used to define areas susceptible to degradation.

In this work, the analyses include applying remote sensing and spatial analysis techniques to estimate soil erosion and land degradation phenomena in abandoned agricultural areas. To emphasize and relate the process of land degradation and soil erosion as negative impacts consequential to land abandonment, it was established to take advantage of a robust methodology, i.e., the Revised Universal Soil Loss Equation (RUSLE) model. Initially adopted to calculate and monitor erosion of small agricultural areas, with the development of new calculation algorithms, this model is now being used to investigate very large areas [50–52]. The study area concerns a district of Basilicata which is particularly vulnerable to land abandonment of arable crops due to the combination of anthropic and natural factors.

2. Study Area

According to many authors, Basilicata, located in Southern Italy (Figure 1), is a region at potential land degradation risk [53–55]. Generally, all the regions of southern Italy are considered at potential risk of land degradation because it derives from a peculiar combination of bioclimatic and geomorphological features such as irregular reliefs with steep slopes, high erodible soils, wide climatic variability, recurring droughts, typical of Mediterranean territories, and from the improper use of soil resources (for example, agricultural overexploitation, urbanization, industrial pollution, etc.) [56]. Basilicata is a mountainous and hilly region characterized by large uninhabited areas. At the same time, 30% of its surface is subject to environmental constraints, highlighting the need for more sustainable land use [45]. Soils are highly susceptible to degradation, e.g., in the coastal area of the Metapontum Plain, soils are degraded due to salinization processes.

In contrast, in the so-called Matera Hills, morphologically complex forms are called *calanchi* (badlands), characterized by irregular erosional processes exposed to strong climatic oscillations and a complex geochemical composition [57,58]. The area investigated in this work includes the territory of 18 municipalities and an extension of about 1600 km². Hydrogeological instability also affects the area; in fact, the IFFI (Inventory of Landslide Phenomena in Italy) project surveyed approximately 860 landslides in 2014 [59].

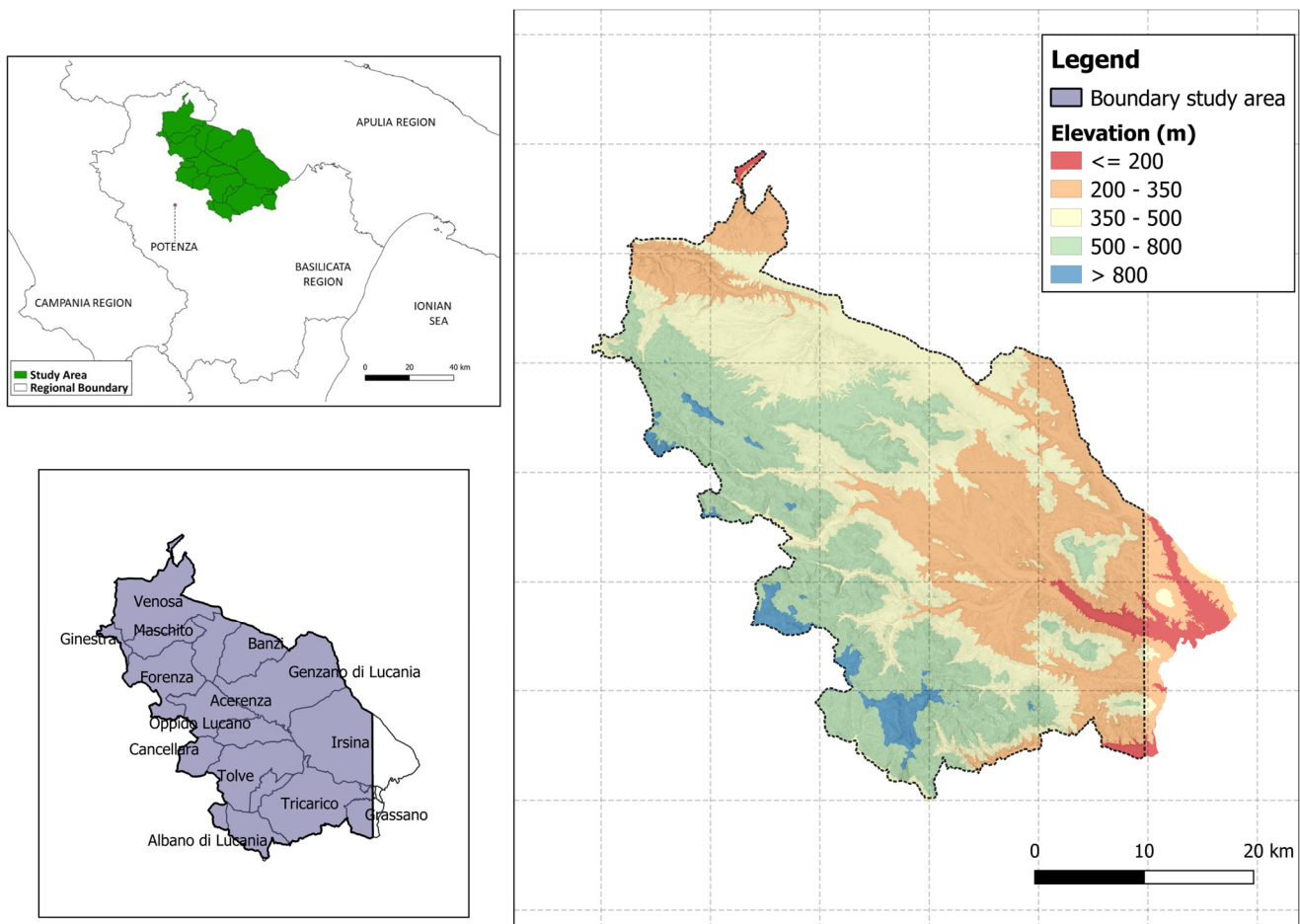


Figure 1. The overall outline of the study area with detail (bottom left) on the part considered in the methodology.

The primary land use is agricultural; from the analysis of land-use data, it can be seen that the area is mainly occupied by agricultural land of different types, primarily arable crops. Considering arable land, heterogeneous agricultural surfaces, permanent crops, stable meadows, and agricultural land uses cover approximately 80% of the entire surface analyzed. The solid agricultural vocation, with an important tendency towards agricultural abandonment [17] and the consequent degradation and erosion processes, make these areas particularly interesting to analyze. Using the Corine Land Cover at level II 2018 [60] as the reference land cover map, we can divide the study area into two main zones according to the predominant type of land use (Table 1).

Table 1. Land cover based on Corine Land Cover II Level expressed in km² and percentage (%).

Corine Land Cover 2018	km ²	%
Agricultural Areas	1266.186	81.45
Artificial Areas	12.44	0.8
Forest and Seminatural Areas	27.4	17.46
Water Bodies	3.772	0.24
Wetlands	0.799	0.5
Total	1554.597	100

The western part is characterized by agricultural areas with complex morphology and is the most diversified from the point of view of land cover because agroforestry patches

can be found. With a gentler morphology, the remaining part presents almost exclusively an agricultural use (mainly arable land).

3. Materials and Methods

To provide a more fluent understanding of the approaches, techniques, and analyses performed, several parts of the paper are summarized and briefly described below:

- Evaluation of soil loss (monthly and annual from October 2019 to September 2020) using RUSLE modeling in the areas subjected to agricultural abandonment;
- Clustering of the results deriving from the application of the RUSLE model by spatial autocorrelation analysis (autocorrelation algorithm Getis & Ord.) to highlight areas with permanent erosion;
- Estimating the susceptibility to soil degradation of arable land and abandoned agricultural areas based on the average values of the RUSLE and mapping of the areas still vegetated but showing signs of degradation, including arable land, through the statistical correlation with the C Factor of the RUSLE.

3.1. Dataset

Satellite images are very useful for constructing land characterization models, risk assessment, and for the susceptibility of soils to erosion. The remote-sensing data used in this work are part of the ESA's Copernicus Mission. Specifically, the data used are from the Sentinel 2 satellite, and the spatial coverage provided by the satellite swatch determined the extent of the study area (Figure 1). Sentinel 2 satellite data provide high-resolution multispectral optical imaging at spatial resolutions between 10 m and 60 m. In this paper, Sentinel data used for determining the C factor of the RUSLE model were downloaded from the THEIA site [61]. The images available on the THEIA site [61] re-process the Sentinel 2A and 2B pair images, with the aggregation of atmospherically corrected TOA bands using the MAYA (Multi-sensor Atmospheric Correction and Cloud Screening) algorithm. The set of bands available at the site is FRE (flat reflectance) and SRE (surface reflectance). In this work, the FRE (Flat Reflectance) bands were used, which, in addition to being atmospherically corrected, suppress reflectance variation due to slope. For images with cloud cover, the algorithm calculates relative masks with two resolutions at 10 m and 20 m. The CLM (Cloud Mask) band at 20 m was used in our case. Twelve images (one for each month) were used from October 2019 to September 2020.

The land cover classification was based on the Corine Land Cover 2018 (CLC) dataset and, for the spatial and statistical analyses, on the 2013 Natura Map on a scale of 1:50,000 in a format freely available at the ISPRA [62] repository in the form of a shapefile. Furthermore, for estimating the parameters of the RUSLE model, in addition to data from the Sentinel satellite and meteorological data, the 'European Soil Map' [63] and the Basilicata Soil Map were used.

3.2. Erosivity Estimation

Soil-loss estimation was estimated using the RUSLE by resampling all necessary parameters to the spatial resolution of Sentinel 2A (10 m) in a GIS environment.

Among the main models for estimating soil erosion, the RUSLE model is one of the most widely used to predict, for example, the annual loss of soil [31,64–66]. RUSLE describes how climate, soil characteristics, topography, and land use influence soil erosion caused by the impact of surface runoff [35]. The RUSLE is based on five variables in Equation (1) related to rainfall patterns, soil properties, topography, crop cover, and management, and conservation tillage practices:

$$A = R * K * LS * C * P \quad (1)$$

where A = annual soil loss ($\text{Mg} \cdot \text{ha}^{-1} \cdot \text{year}^{-1}$); R = precipitation erosion factor ($\text{MJ} \cdot \text{mm} \cdot \text{ha}^{-1} \cdot \text{h}^{-1} \cdot \text{year}^{-1}$); K = soil erodibility factor ($\text{Mg} \cdot \text{h} \cdot \text{MJ}^{-1} \cdot \text{mm}^{-1}$); LS = slope length

and slope factor (dimensionless); C = crop and cover management factor (dimensionless); and P = crop or erosion control factor (dimensionless). The result estimates the amount of soil lost due to surface erosion. All parameters calculated were resampled to the spatial resolution of Sentinel-2A (10 m) and summed to obtain the actual value of RUSLE expressed in $\text{Mg} \cdot \text{ha}^{-1} \cdot \text{year}^{-1}$. The RUSLE values were calculated for the following months: October, November, and December 2019 and March, April, May, June, July, August, and September 2020. For the monthly RUSLEs, a specific model has been implemented by the Graphical Modeler of QGIS to realize batch processing and calculate the different parameters semi-automatedly. Finally, the monthly values were summarized to have an annual RUSLE value. The months of January and February 2020 were not included in the calculation of RUSLE because cloudless satellite imagery is not available for C -factor estimation.

3.2.1. Rainfall Erosivity Factor (R)

Rainfall has the most significant erosive impact among the various climatic factors that characterize a territory. The precipitation erosivity factor R is an average index that measures the kinetic energy and intensity of precipitation to describe the effect of erosion, two parameters that significantly influence erosive processes. R indicates the quantity of rainfall and peak intensity of the rainstorm that determine its erosive power. Soil loss from cultivated fields is related to the energy and intensity of each rainfall in that area [30].

From the online database of the Functional Centre of the Basilicata Region [67], the cumulative monthly rainfall data of six meteorological stations (Albano di Lucania, Irsina, Venosa, Palazzo San Gervasio, Oppido Lucano, and Grassano) were downloaded.

The R -factor equation is based on the rainfall intensity developed for the Basilicata region in the work of Capolongo [68], in which only daily rainfall contributions with values greater than ten are added up.

$$R = 0.1087 * \left[\text{daily cumulate rainfall}^{(1.86)} \right] \quad (2)$$

Once the point values of R were obtained for all months of the period considered for each rain gauge, the data were spatialized using interpolation tools, thus obtaining a probable erosivity factor R for the entire study area.

3.2.2. Soil Erodibility Factor (K)

The soil erodibility factor K is the rate of soil loss per unit of the rainfall erosion index ($\text{t ha h ha}^{-1} \text{ MJ}^{-1} \text{ mm}^{-1}$) as defined by Terranova [69]. The factor K is the long-term average response of soil and soil profile to the erosive power of storms. In particular, it represents the detachment and transport of part of the soil components due to rain- and surface-flow impact. It considers specific characteristics of the soil components, from abrasive effects due to transport and localized deposition of soil parts depending on the topography to rainwater infiltrations in the soil profile [27].

$$K = \left[\frac{2.10 * 10^{-4} * (12 - M) * [(Si + fS) * (100 * C)]^{1.14} + 3.25 * (A - 2) + 2.5 * (P - 3)}{100} \right] \quad (3)$$

M represents the organic matter, expressed as a percentage (%), present in the soil, Si is the percentage of silt from 0.002–0.05 mm, fS is the content of very fine sand with a diameter 0.05–0.1 mm, and C is the percentage of clay with a diameter <0.002 mm. The K values thus obtained were multiplied by the factor 0.1313 to be expressed in the unit of the International System. The parameters were derived from the Pedological Map of the Basilicata Region and the Basilicata Region soils database to define the factor on the area under investigation.

3.2.3. Topographic Factor (LS)

The L and S factors represent the effect of topography on soil erosion rate and are the most difficult factors to determine in the RUSLE equation due to the topographic variability

of the areas investigated [70]. Slope length (L) in RUSLE is defined as the distance from the point where surface flow begins to the point where storage occurs, or runoff waters are channelized. The topographic factor comprises slope length (L) and slope steepness (S).

Soil loss increases if the slope length increases due to downward runoff accumulation. Slope (S) describes how erosion increases with the slope angle. Soil erosion increases with the slope angle due to runoff's increasing velocity and erosivity [71]. Many authors have developed equations to estimate the LS factor [66,69,72–74]. The formula proposed by Mitasova [75,76] was used to calculate the topographic LS factor relative to a point r on a hillslope, which includes into a single factor LS the parameters relating to slope length L and slope S , using a formulation that better interprets the topographical complexity of the examined region:

$$LS_{(r)} = (\mu + 1) \left[a_{(r)} / a_0 \right]^\mu \left[\sin b_{(r)} / b_0 \right]^n \quad (4)$$

where $a_{(r)}$ is the upslope-contributing-area per unit contour width, in this study assessed by the product of QGIS with GRASS function $r.flow$, b is the slope, μ is the slope length exponent [77], n is a parameter whose value has been set to 1.2 [69], $a_0 = 22.1$ m is the standard USLE plot length, and $b_0 = 9\%$ is the slope grade of the standard USLE plot. The LS factor was estimated using the 20 m gridded DEM with the support of QGIS software; in fact, most LS estimation algorithms are implemented within GIS software. The LS product factor is dimensionless and was assumed constant over the entire observation period [75].

3.2.4. Crop Management Factor (C)

The C Factor is non-dimensional and is calculated to consider a vegetation cover's impact on erosion. Several papers in the literature C [31,65,66] have different approaches to estimating the C Factor, which can differ depending on the other parameters considered. C depends on many sub-factors, such as vegetation cover, soil moisture, and foliage residue, which change continuously throughout the year, so it is necessary to be able to estimate an indicator to calculate the state of vegetation both spatially and over time. The SAVI [78,79] vegetation index was used to estimate the C-Factor Equation (5).

$$SAVI = \frac{[(NIR - RED) * (1 - L)]}{(NIR + RED + L)} \quad (5)$$

The equation, defined by Kuo et al. [79], was used to calculate the C Factor:

$$C = -a * SAVI + 1 \quad (6)$$

where a is the land cover management factor to which value 1.18 was assigned. The C Factor will have values between 0 and 1; where 0 indicates complete coverage vegetation cover and 1 indicates no vegetation cover or bare soil. Therefore, a value of C close to zero is indicative of soil not exposed to erosion, while high values of C are indicative of soil exposed to erosion [80]. According to Alejandro [81], estimating the C Factor becomes more complicated depending on how land use and vegetation change. The estimation of C using satellite vegetation indices could effectively respond to continuous and rapid changes in vegetation and land use.

In the estimation of the C Factor, among the vegetation indices, NDVI is among the most widely used, according to Lin [82], there is a linear correlation between the C Factor and NDVI, and other authors, such as Van der Knijff [83], presented a C-factor equation based on the NDVI index, as applicable in Europe.

Lin also observes that the NDVI is highly variable and, therefore, would decrease the accuracy in calculating C . For this reason, the Soil-Adjusted Vegetation Index (SAVI) presented by Huete [84] is the most suitable for a better estimate of C [85,86].

3.2.5. Conservation Support Practice Factor (P)

The factor relative to conservation practices (P) provides the ratio of soil loss of supporting practices and is used to quantify the positive impacts of these practices.

The P factor considers control practices that decrease the erosive potentials of runoff due to their influence on drainage patterns, runoff concentration, and runoff velocity. The value of the P factor varies from 0 to 1, with a value approaching 0 indicating good conservation practice and a value approaching 1 indicating poor conservation practice [30]. The P factor was derived from a dataset freely available online on the ESDAC website [87].

3.2.6. Clustering of RUSLE Values

Integrating satellite imagery and geostatistical analysis is a very innovative approach for analyzing and mapping those factors that are spatially variable. In the study of statistical variables representative of phenomena or processes acting at the land scale, the issue of spatial autocorrelation is crucial in assessing whether a particularly intense phenomenon in a specific area implies the presence of the same in contiguous areas as well [88].

Spatial autocorrelation indices were applied to monthly and annual soil erosion maps obtained from applying the RUSLE model.

The concept of spatial autocorrelation is one of the most important in spatial statistics. It derives from the first law of geography introduced by Tobler in 1970 [89], “everything is related to everything else, but near things are more related than distant things.” Auto-correlation indicators measure whether and how much a dataset is autocorrelated across the study region. Similar values of the variable result in spatial clusters in the presence of positive spatial autocorrelation. In the presence of negative spatial autocorrelation, spatially clustered different values of the variable are present; the absence of spatial autocorrelation indicates a random distribution of values in space. After applying several indices to the monthly RUSLE values, the choice fell to using the G_i local autocorrelation index proposed by Getis and Ord [90,91]. Getis and Ord’s algorithm is a local indicator of spatial autocorrelation; local indicators allow us to identify clustered pixels, measuring how homogeneous the features within the area are. In particular, a high index value means a positive correlation for high-intensity values, while a low value of the index means a positive correlation for low-intensity values.

In applying autocorrelation methods, it is important to define the nature of the events investigated and the geometric relationships involved. In image processing, the spatial event is associated with a pixel, and spatial autocorrelation statistics are usually calculated by considering the geographic coordinates of its centroid [88].

Intensity, on the other hand, should be chosen by strictly considering the empirical nature of the case study. The conceptualization of geometric relationships in the case of image processing is very simple because the distance between events is always equal or is a multiple of the pixel size. The application of spatial autocorrelation statistics to remote sensing images allows us to obtain a new raster that contains in each pixel a number expressing how much it is autocorrelated to another pixel.

Given the study’s objective, the intensity is given by the erosion and, thus, by the RUSLE values. In this document, we have used as intensity (G_i of Getis and Ord) the value of RUSLE calculated using Equation (1).

The latter technique was applied individually to each month, highlighting only the pixels with positive autocorrelation and then cumulating into a final raster, allowing the development of a map indicating areas that exhibit a permanent erosion rate.

3.3. Identification Areas Susceptible to Degradation

To study the process of soil erosion on a large scale in as much detail as possible, it was decided to deploy an additional method referring specifically to rural and agricultural abandoned areas. Erosion susceptibility of erosion events is based on their spatial distribution under the influence of specific causal factors [92,93]. Logistic regression is a frequently applied multivariate statistical technique for modeling susceptibility by investigating the

interactions between erosion factors. In the literature, in the absence of a scientific framework on the subject, the susceptibility analysis needs to improve on the subjectivity of researchers in choosing the factors to use [94,95].

This new analysis approach is based on factors included in the RUSLE model, particularly on the relationship between some of these factors and the overall erosion index, to identify the most susceptible areas to the effect of degradation [38]. To examine the problem of erosion in agricultural areas (particularly arable land and abandoned agricultural areas), the C Factor was referred to because it is the factor that assesses the influence of agricultural land-use management on the erosion factor (A). Land covered by vegetation is more protected from erosion because the leaf area present provides a physical barrier to the impact of rainfall and the sliding effect of debris downstream. Identifying areas where erosion is high, primarily during periods of vegetation growth, implies that those areas have evident problems caused by poor vegetation cover. Therefore, by isolating RUSLE's C Factor and linking it to RUSLE's A during periods of maximum vegetation activity, it is possible to obtain and identify areas subject to probable degradation as they show a high erosion rate despite the soil being covered by vegetation. March was investigated because it is the period when the land is mostly covered by vegetation, and the arable land's phenological stage is crucial. To show how the C Factor influences the A factor in relation to the other parameters, we set the slope factor (for the morphological part) and the R factor (for erosivity due to precipitation) in a range of three classes. A table of combinations can be constructed based on the class of each factor, as shown in Figure 2.

The diagram in Figure 2 describes the steps to identify degraded areas, starting with examining the RUSLE factor. For each combination of the slope classes and the R factor, A value was selected only for abandoned agricultural areas and arable land belonging to the Nature Map of ISPRA, thus obtaining nine distinct layers in the ranges of slope and R erosivity referred to March 2020.

Since the objective is to look for the correlation between the erosivity of the A factor and the C Factor, it was chosen to compare them through the analysis of linear regression by the map of residuals for each $\text{regr}[A_{(i,j)}, C]$ pair. The residual maps $A_{\text{res}}(i,j)$ quantify, pixel by pixel, the error ε calculated on the difference between the value of estimated A and the actual A. The direct proportionality $Y = AX + B + \varepsilon$ is given by the points closest to the regression line and thus the points at which the value of residuals ε is small in absolute value. In order to select the values of A where the error can be considered minimal, a threshold $\varepsilon = |Y_{\text{Real}} - Y_{\text{Estimate}}| < 2$ was defined around the regression line to highlight all points that fall therein and to identify areas instead of only recurring to points that lie right on the line. The pixels thus obtained will be characterized by a large and direct proportionality because they are close to the line as opposed to the more distant pixels, which, instead, do not give proportionality and consequently are not of interest to our analysis. In defining the areas where the vegetation factor weighs more on the value of A, all other things being equal, to define those showing a high erosion value, a threshold was placed on each layer $A_{\text{res}}(i,j)$, excluding all pixels with values less than or equal to $5 \text{ Mg/ha}^{-1} \cdot \text{year}^{-1}$. The result represents those areas that, despite being covered by vegetation, have a high erosion factor. In these areas, erosion could cause or already is causing low productivity and is destined for abandonment. The nine $A_{\text{res}}(i,j)$ maps were combined successively to compose a single map of areas of degradation.

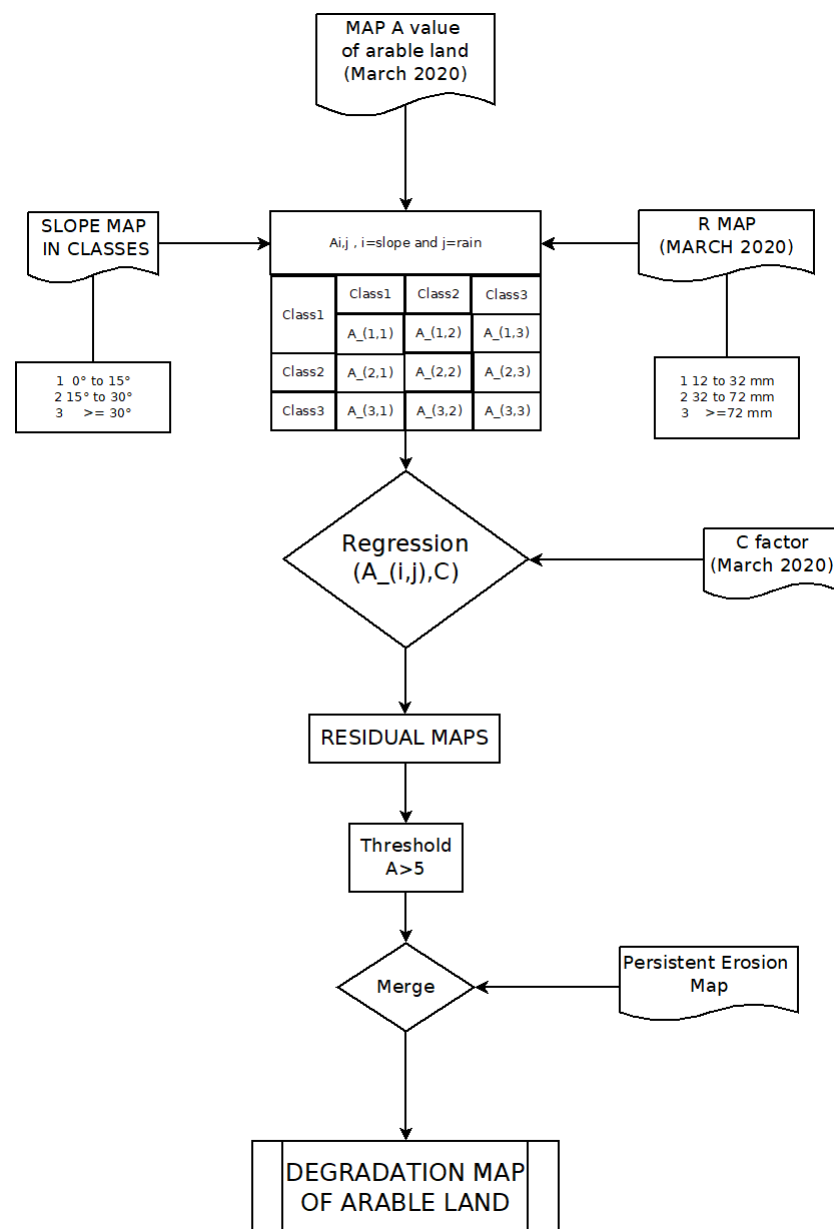


Figure 2. Flow chart for the elaboration of a degradation map of rural land.

4. Results and Discussions

4.1. Persistent Erosion Map

The final results identified and estimated the average annual soil loss and erosion-susceptible zones in the study area.

The development of the RUSLE model involves the generation of an intermediate raster representing the different processes that may influence, to different degrees, the overall erosion of soils. For a more accurate analysis, each factor should be evaluated individually to examine how each influences and weighs on the final value of the RUSLE.

One of the most important factors related to R is the rainfall erosivity. The first contribution of rain to erosion begins when raindrops touch the soil, leading to what is known as an “erosion splash.” According to the energy and properties of the raindrops and the soil on which they fall, a specific type of soil particle separation may occur [28]. Later, when the event is so powerful that not all the water infiltrates into the soil, partially due to the low soil permeability, water that does not infiltrate but accumulates on the soil starts to flow following the direction of maximum slope and cutting larger and deeper channels

(rills and gullies). Kinnel, in 2005 [96], stated that particle detachment occurs when the erosive forces of raindrops and water flow overcome the soil’s resistance to erosion.

The result of Inverse Distance Weighting (IDW) [97] interpolation using cumulative rainfall data from six meteorological stations (Albano di Lucania, Irsina, Venosa, Palazzo San Gervasio, Oppido Lucano, and Grassano) showed that the average monthly rainfall ranges from 11.11 mm to 222.70 (MJ*mm/ha*h*year). Figure 3 shows the mean values of the R factor during the observation period of October 2019–September 2020; the highest values occurred during November 2019, followed by March 2020 and July 2020.

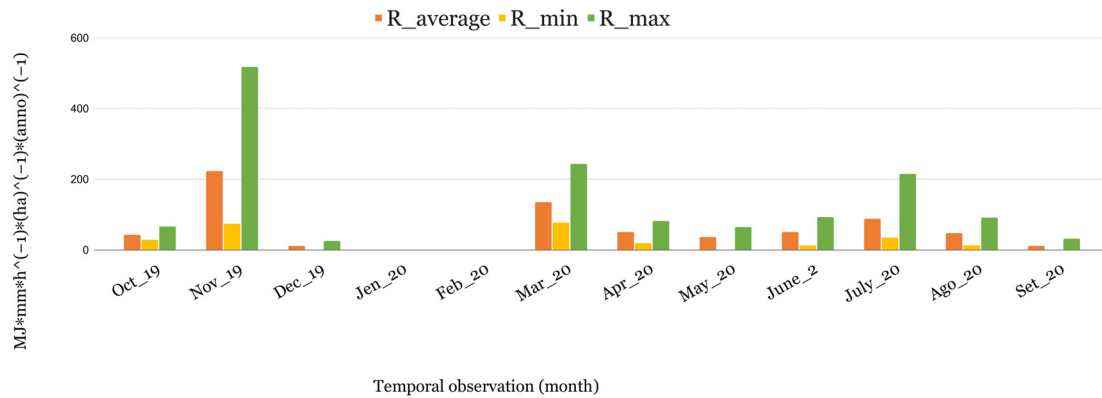


Figure 3. Histogram of the trend in R values during the months of analysis (October 2019 to September 2020).

The C Factor is related to the vegetation cover of the investigated area; it is related precisely to the vegetation growth and development factors of the entire observed period, in this case, one year. For this reason, the histogram in Figure 4 shows different values during the whole period. The highest values are recorded in the summer because the investigated area shows predominantly agricultural areas, and post-crop land use shows very low vegetative cover. In the autumn months (October and November), high C values are observed. Still, in this case, the higher-than-average value considers the absence of vegetative cover in natural areas.

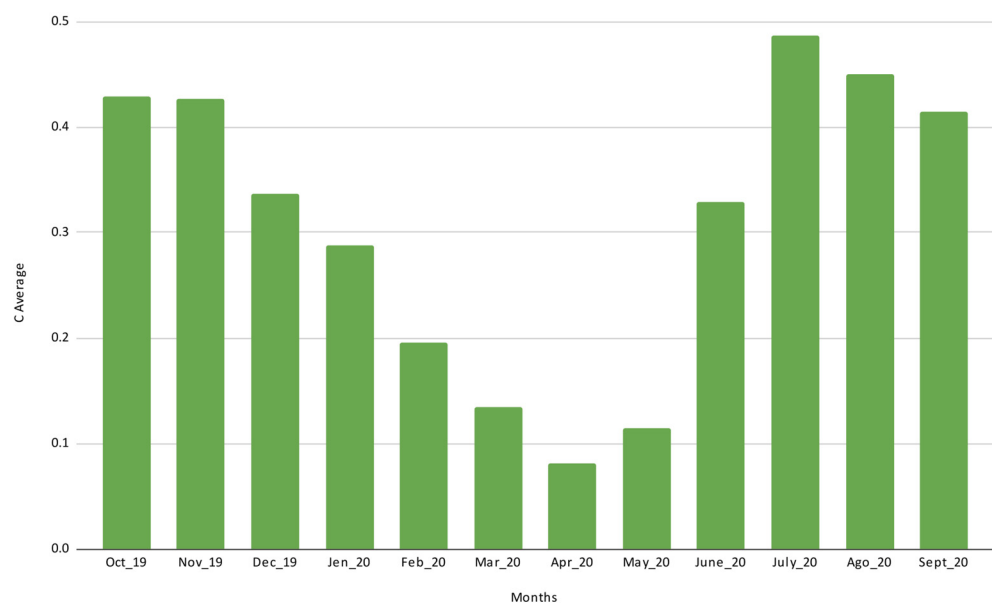


Figure 4. Histogram of the C values trend during the months of analysis (from October 2019 to September 2020).

To estimate monthly RUSLE values (Figure 5), the computational process was automated by creating Graphical Modeler QGIS software to perform batch processing to estimate the different parameters semi-automatically. January and February 2020 were not included in the RUSLE calculation because the satellite imagery had cloud cover and could not be used in the C-value estimation. Subsequently, erosion data obtained from the RUSLE calculation were compared and correlated with land-cover data to assess how this process may influence degradation phenomena and the relationship with agricultural abandonment. A preliminary study was based on the results of monthly and annual average values of RUSLE concerning mainly arable farmland and abandoned farmland.

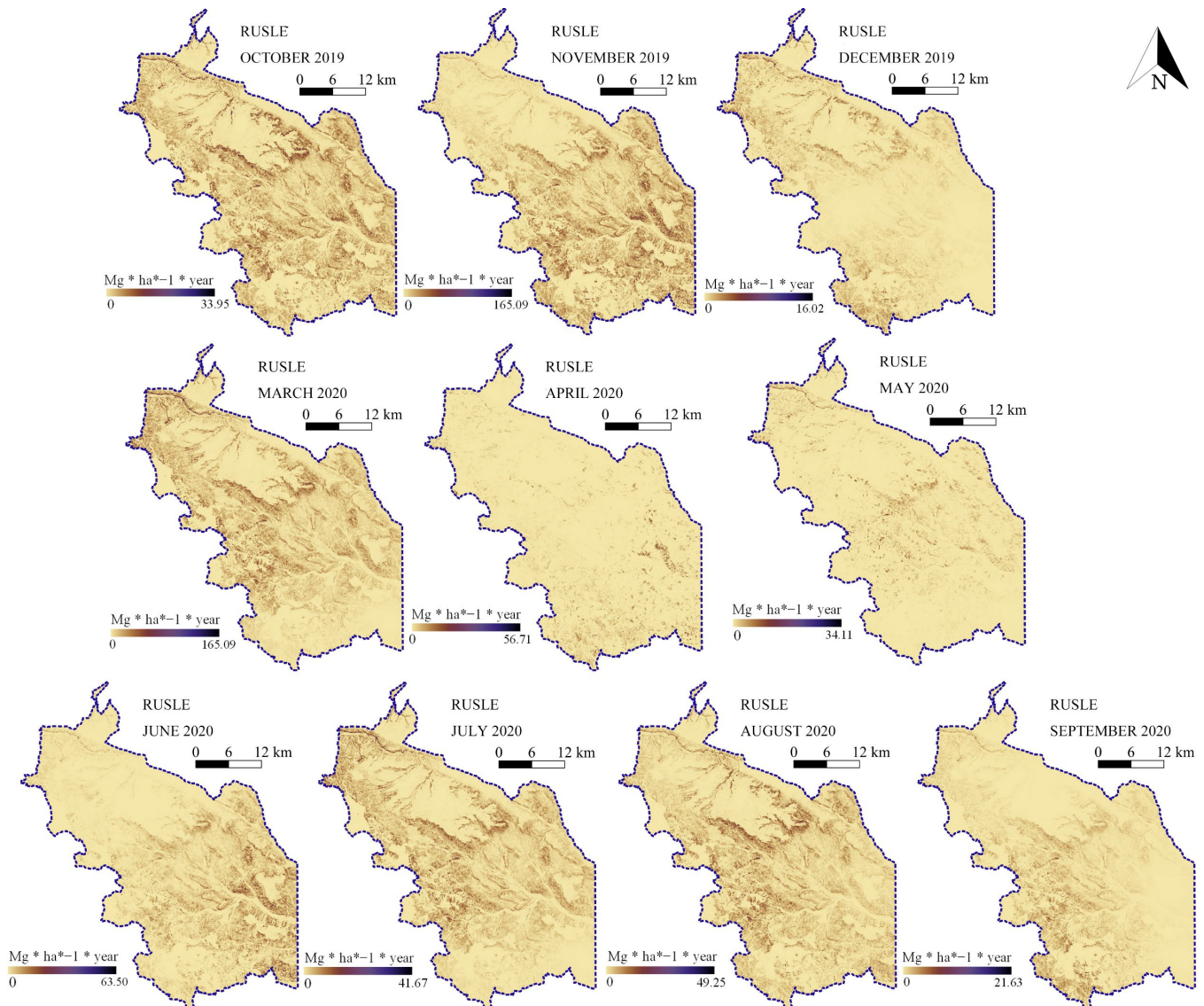


Figure 5. Example of the results of the parameters used for calculating the RUSLE. For R and C Factors, only one monthly run was reported as an example.

Analyzing the annual values of RUSLE, Table 2 shows that the erosion rate is marginally higher in abandoned areas with typical post-crop vegetation (abandoned lands). Borrelli compared erosion data and different types of land use, identifying a significant drop in the estimates of soil erosion rates from cultivated lands to forests and other forms of semi-natural vegetation [98]. In this study, agricultural areas covered about 11% of the areas studied and are responsible for about 50% of the overall erosion. The authors estimated that agricultural areas had, on average, considered rates of erosion times that were higher

than the overall rate of soil erosion throughout the year of the study. It is also estimated to be about seven times higher than the average erosion of soils with natural vegetation cover [98].

Table 2. Average monthly and annual RUSLE values (expressed in $Mg\text{-ha}^{-1}\text{-year}^{-1}$) for arable and abandoned lands.

Period	Abandoned Lands	Arable Lands
October 2019	1.81	2.10
November 2019	8.81	8.84
December 2019	0.42	0.34
March 2020	7.22	3.94
April 2020	0.90	0.35
May 2020	0.37	0.39
June 2020	1.95	2.19
July 2020	1.85	1.96
August 2020	2.29	1.33
September 2020	0.69	0.48
YEAR (2019–2020)	26.23	22.92

In this work, the difference in the amount of erosion in areas with different land cover types is extremely important to investigate because high erosion values are mainly found in arable agricultural areas where several months of the year have bare soil.

The reason could be that areas with post-crop vegetation have a higher land cover type (expressed by the RUSLE C Factor) and morphological context that could influence erosion.

The months with the highest average values are November 2019 and March 2020 (Table 3). Overall, land use/cover classes with the highest average annual values are those of clayey areas subject to strong erosion; badlands are known to suffer the effects of erosion due to the almost absence of vegetation and their geological and pedological features [99,100]. The average erosion values are highest in areas where vegetation species, typical of post-crop processes due to the abandonment of arable land, are present.

Table 3. Surfaces in hectares and as a percentage of areas in permanent erosion.

Land Cover Classes	Hectares (ha) in Persisten Erosion	% of Total Persistently Eroded Area
Arable Land	493.96	22.48
Abandoned Area	1343.11	61.13
Olive groves, vineyards and orchards	143.89	6.55
Forests and shrublands	29.57	1.35
Riparian vegetation areas	18.52	0.84
Gully areas	149.48	6.80
Urban areas, quarries, industrial sites	18.76	0.85

These areas are included in the classes marked by species and ecological successions typical of areas where agricultural activities (cereal cultivation and/or grazing) have been interrupted for some time and with some temporal continuity. Concerning t classes related to crop abandonment, all show average values above the total annual value. Areas covered by forests may also show erosion problems in particular contexts (e.g., overgrazing in steeply sloping areas, inappropriate cutting in the past, and fires).

The study area is covered by about 9% of areas showing post-crop vegetation derived from agricultural abandonment. These areas are prevalently located in the western and south-western sides, involving zones with different morphological characteristics, soil types, and socio-economic conditions, and are less profitable for intensive agriculture.

Focusing on arable land, it can be seen that the month showing the most significant values is November 2019. This is due to the amount of rainfall that has decreased and also to the fact that in November, arable land has no vegetation cover, as it is the transition period between the end of the agricultural year and the beginning of planting for the next one. Since there is no vegetation cover, March is optimal for studying land degradation due to erosion in arable land.

Erosion is determined in November, with the R parameter of RUSLE being equal due to rainfall, only by the stationary factors K and LS. This is called “natural potential” [101], which does not consider the influence of vegetation. Areas, where high erosivity values emerge can be indicated as those areas subject to greater susceptibility to soil degradation and, therefore, should receive more attention.

Abandoned areas present higher erosion values in the periods of November and March. Compared to arable areas, November exhibits lower values, despite the difference in land use in the two land cover types. There could be many reasons for this, but they require further investigation as several factors could be involved, related to morphological and physical factors as well as different stages of abandonment. In March, the average erosion value in the abandoned areas is almost twice compared to those found in arable land, presumably because in this month, the cultivated areas already provide some degree of land cover, and the herbaceous and shrub vegetation has not yet, as the growing season starts later than that of cereals and other arable crops.

Applying the local autocorrelation algorithm of Gi has allowed us to identify the areas to pay attention to, characterized by permanent erosion, which takes into account the spatial and geographical relationships that may exist between contiguous areas emerging from the monthly RUSLE calculations. The pixels marked in the map are spatially and geographically related to each other, according to the intensity of the monthly RUSLE value (Figure 6).

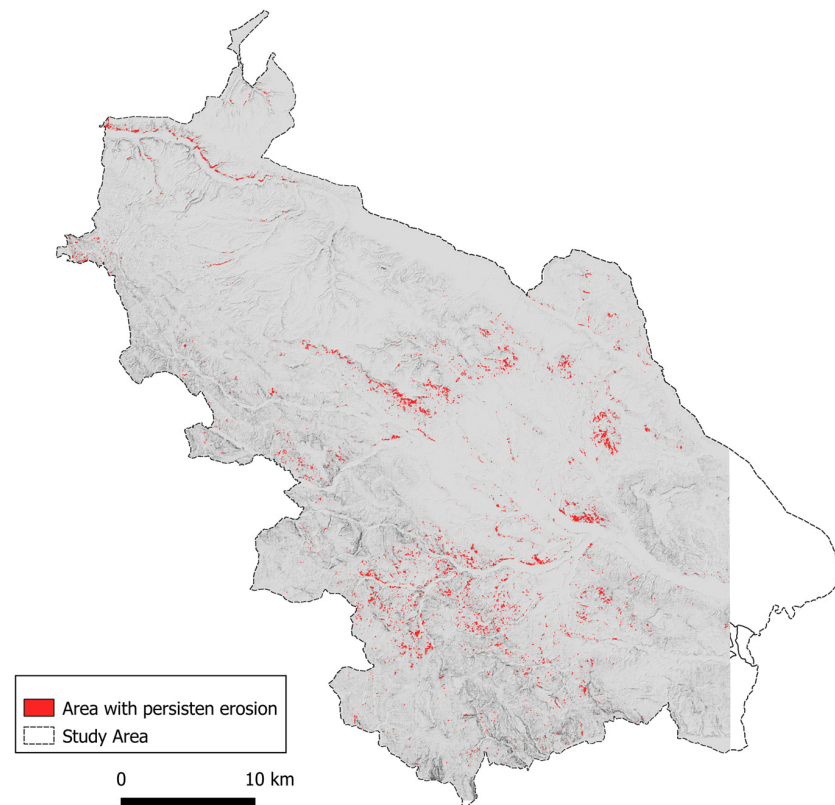


Figure 6. Map of permanent erosion between October 2019 and September 2020.

Pixels have been reclassified only to have discrete values 0–1. The areas showing persistent erosion rates have value one and correspond to those in the analyzed period with positively autocorrelated RUSLE values. These areas have a constant erosive contribution during all the analyzed months. To interpret this process more clearly, results were correlated to land cover to evaluate which classes were most affected by permanent erosion in terms of surface area. The most significant classes (Table 3) relate to arable land and abandoned agricultural areas. Furthermore, by relating the hectares in permanent erosion to the total area of the land cover class, it is possible to identify those areas most affected by a higher erosion rate each month. From this analysis, it can be seen that the highest rates are found in classes that, due to their characteristics, are subject to erosion phenomena (gullies, quarries, and riverbeds); the classes of land use are subject to agricultural abandonment processes that follow.

Spatial statistical analysis indicates that arable land and abandoned areas have significantly higher erosivity rates, with the last representing more than 61 percent. The results of these activities made it possible to produce preliminary land degradation susceptibility maps for arable and abandoned land. The mapping outputs make it possible to identify large areas or clusters that need to be monitored because they may be susceptible to degradation.

The actually cultivated areas could be susceptible to degradation as they have higher erosion values than average ones in March 2020 and variable but permanent erosion throughout the year analyzed. Moreover, these areas predominantly show cereal crops. They are therefore subject to significant periods of the year when the soil is bare and are also subject to different types of mechanized tillage, exacerbating the vulnerability of these plots. Regarding the areas with post-crop vegetation resulting from abandonment processes, elaborations of areas susceptible to land degradation were evaluated based on the RUSLE values obtained for November 2019.

4.2. Mapping of Sensitive Land Degradation Areas

This section presents the results of evaluating erosion variables and the susceptibility analysis.

The multiple regression analysis technique is used to predict the response (dependent) variable based on two or more predictor (independent) variables [92,102]. This technique is used to evaluate each predictive variable's contribution to the model's total variability. It can also be applied to validate the variability of the response variable by adding new predictive variables to the model. This type of analysis has advantages and disadvantages, which are widely described in the literature, where many examples can be found [103–105].

In this study, the predictor variables (i.e., RUSLE parameters: R, LS, and C) are grouped into static and dynamic factors, while the response variable is actual soil loss (A RUSLE).

The areas analyzed in March 2020 represent areas where erosion strongly correlates with the C Factor. To define with a reasonable probability that these are year-round, it is necessary to integrate the data with the Getis map of the entire area, obtained by spatial autocorrelation, which covers the areas subject to permanent erosion from October 2019 to September 2020. As an end result, the intersection provides a soil degradation map for arable land that shows high RUSLE values during the growing season and keeps them throughout the year. The map in Figure 7 and Table 4 summarizes the result obtained from the realization of the map of agricultural areas (cultivated and abandoned) strongly correlated to the vegetation factor C, susceptible to degradation.

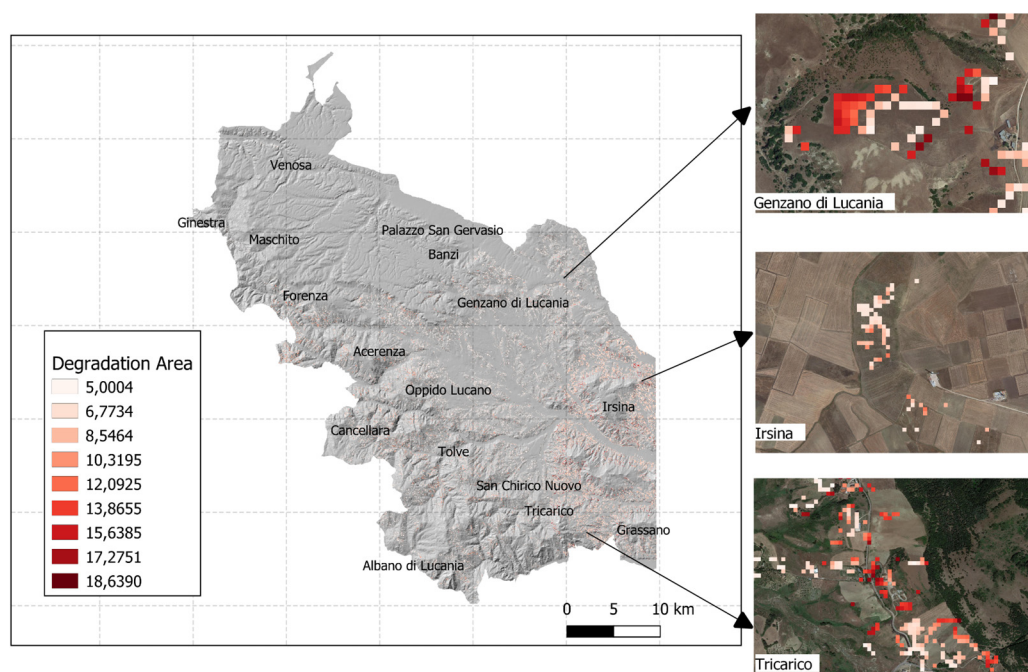


Figure 7. Map of degradation areas.

Table 4. Extension of the areas subject to degradation cultivated with arable land in degradation concerning the factor C.

Municipality	Degradation (ha)	RUSLE (A) Average	Degradation Area (%)
Tolve	70.32	7.37	0.97
Genzano di Lucania	63.48	6.95	0.35
Tricarico	36.20	9.07	0.42
Irsina	19.48	8.58	0.13
Forenza	14.72	7.33	0.23
Acerenza	13.00	6.87	0.29
San Chirico Nuovo	12.52	7.65	1.49
Venosa	6.44	5.79	0.05
Banzi	3.08	6.46	0.05
Oppido Lucano	2.68	6.71	0.07
Ginestra	2.24	5.94	0.42
Cancellara	2.12	7.61	0.10
Palazzo San Gervasio	1.68	6.93	0.04
Albano di Lucania	0.76	7.74	0.05
Maschito	0.48	5.57	0.01
Grassano	0	0	0

The municipalities within the study area are shown in the table's first column; the surface, in hectares, of degraded agricultural areas per municipality is indicated in the second. The following column shows each municipality's average value of erosion of the degraded areas. Finally, the area calculated with the methodology and the agricultural area relating to each municipality were compared.

Tolve has the most degraded hectares, with an average A of 7.36 [$\text{Mg}\cdot\text{ha}^{-1}\cdot\text{year}^{-1}$] and a percentage of the total area of around 0.97%. Another interesting fact to highlight is the area of San Chirico Nuovo, which has the highest degraded area of 1.48% with an average erosion of 7.65 [$\text{Mg}\cdot\text{ha}^{-1}\cdot\text{year}^{-1}$]. The data referring to the municipalities of Irsina and Grassano is partial because the study area only includes part of the municipal territory. Figure 8 shows in detail some areas that show high susceptibility to degradation.

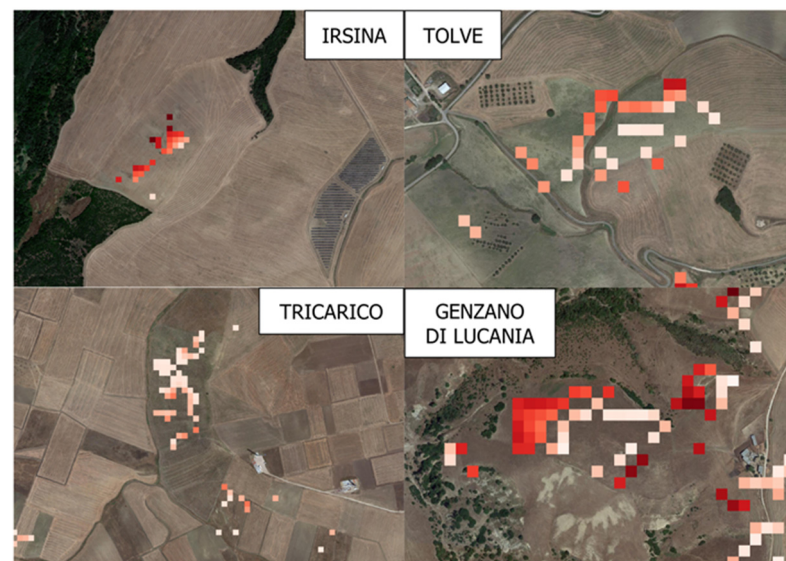


Figure 8. Detailed examples of areas subject to land degradation on arable land in four different areas.

For overlapping pixels (Figure 8), the orthophoto identifies the clusters where land degradation is most likely to occur. There may be a variety of causes for this process, one of which could be, for example, intensive exploitation (excessive mechanization and use of chemicals), resulting in the loss of organic content that leads to the deterioration of soil structure, thus facilitating the initiation of erosion.

Land degradation susceptibility estimation measures the likelihood that soil erosion will occur in a location based on the relationship between its past and various causal factors [92,102]. In the multivariate statistical model, all erosivity parameters (independent variables) responsible for erosion were treated together, and their interactions helped to determine the future probability of land degradation [106]. The model also assessed the relative contribution of each variable, placing more emphasis on variables known to contribute to erosion occurrence. Logistic regression analysis was chosen as the appropriate multivariate technique due to the nature of the data used in this study [106].

The independent variables used in this analysis include non-continuous data (slope angle, C Factor, and rainfall data). The dependent variable is binary (presence or absence of erosion). Detailed descriptions of the technical logistic regression can be found in the literature [107,108].

Independent variables were gradually entered into the process if their probability of remaining in the model was more significant than 5 (the default cutoff for this case study). The results were then transferred to the QGIS Raster Calculator for the probabilistic development of the land degradation–erosion susceptibility map (pixel size 20 m × 20 m). The susceptibility map has been classified into several classes, from the lowest values indicating a low probability of degradation to progressively higher values.

5. Conclusions

The abandonment of agricultural land is one of the most important manifestations of changes in the use of cultivated land. It is difficult to explain the negative impacts of a complex and spatially variegated process, such as agricultural abandonment [109,110]. Throughout this study, land erosion related to water action was considered a parameter closely related to land degradation due to agricultural abandonment. This study provides a first insight into the impacts linked to agricultural land abandonment in the municipalities analyzed. The adopted analyses have made it possible to evaluate the relationships between changes in agricultural land use and degradation processes since erosion processes occur more in areas that have undergone changes in land use and/or abandonment. In contrast, in permanent agricultural areas, the impact of the erosion process is generally lower. With the methodologies applied in this study, it was possible to create different datasets, both

tabular and in the form of maps, to evaluate the land degradation process related to land use and land-cover dynamics.

Applying the logistic regression model for susceptibility analysis is appropriate for the present study. The results of this analysis provided information that led to a significant improvement in understanding the spatial distribution of agricultural soil erosion due to agricultural abandonment and/or agricultural overexploitation. The susceptibility maps produced in this study can be used as a guideline for land management in land-use planning. More site-specific testing and analysis are needed to establish the distribution of areas subject to likely degradation. The erosive impact of abandoned and uncultivated land raises important questions about implementing land conservation programs. It is difficult to cooperate with those involved in soil conservation and land degradation prevention activities and to involve farmers whose animals are grazing on unused land. Sustainable rural land use and management through integrated planning could mitigate this ongoing process and avoid negative impacts. Replicable and updatable land planning techniques and methodologies need to be implemented to quantify and analyze the consequences of agricultural abandonment at high levels of detail. This study can be used as a reference for spatial planning policies to achieve the Zero Net Degradation Land objective by 2030 [111].

Author Contributions: All authors contributed equally to this work. Experiment designs and writing manuscripts were developed mutually by all authors. All authors have read and agreed to the published version of the manuscript.

Funding: This research received no external funding.

Conflicts of Interest: The authors declare no conflict of interest. The funders had no role in the design of the study, in the collection, analyses, or interpretation of data, in the writing of the manuscript, or in the decision to publish the results.

References

- García-Ruiz, J.M.; Lana-Renault, N. Hydrological and erosive consequences of farmland abandonment in Europe, with special reference to the Mediterranean region—A review. *Agric. Ecosyst. Environ.* **2011**, *140*, 317–338. [[CrossRef](#)]
- Levers, C.; Schneider, M.; Prishchepov, A.V.; Estel, S.; Kuemmerle, T. Spatial variation in determinants of agricultural land abandonment in Europe. *Sci. Total Environ.* **2018**, *644*, 95–111. [[CrossRef](#)] [[PubMed](#)]
- Arnaez, J.; Lasanta, T.; Errea, M.P.; Ortigosa, L. Land abandonment, landscape evolution, and soil erosion in a Spanish Mediterranean mountain region: The case of Camero Viejo. *Land Degrad. Dev.* **2011**, *22*, 537–550. [[CrossRef](#)]
- Smiraglia, D.; Ceccarelli, T.; Bajocco, S.; Perini, L.; Salvati, L. Unraveling Landscape Complexity: Land Use/Land Cover Changes and Landscape Pattern Dynamics (1954–2008) in Contrasting Peri-Urban and Agro-Forest Regions of Northern Italy. *Environ. Manag.* **2015**, *56*, 916–932. [[CrossRef](#)]
- Saganeiti, L.; Pilogallo, A.; Scorza, F.; Mussuto, G.; Murgante, B. Spatial indicators to evaluate urban fragmentation in basilicata region. In Proceedings of the Computational Science and Its Applications—ICCSA 2018, Melbourne, VIC, Australia, 2–5 July 2018; pp. 100–112.
- Scorza, F.; Pilogallo, A.; Saganeiti, L.; Murgante, B. Natura 2000 Areas and Sites of National Interest (SNI): Measuring (un)Integration between Naturalness Preservation and Environmental Remediation Policies. *Sustainability* **2020**, *12*, 2928. [[CrossRef](#)]
- DLG. *Land Abandonment, Biodiversity and the CAP*; Government Service for Land and Water Management of the Netherlands (DLG): Utrecht, The Netherlands, 2005.
- Leal Filho, W.; Mandel, M.; Al-Amin, A.Q.; Feher, A.; Chiappetta Jabbour, C.J. An assessment of the causes and consequences of agricultural land abandonment in Europe. *Int. J. Sustain. Dev. World Ecol.* **2017**, *24*, 554–560. [[CrossRef](#)]
- Pazúr, R.; Lieskovský, J.; Feranec, J.; O’ahel, J. Spatial determinants of abandonment of large-scale arable lands and managed grasslands in Slovakia during the periods of post-socialist transition and European Union accession. *Appl. Geogr.* **2014**, *54*, 118–128. [[CrossRef](#)]
- Renwick, A.; Jansson, T.; Verburg, P.H.; Revoredo-Giha, C.; Britz, W.; Gocht, A.; McCracken, D. Policy reform and agricultural land abandonment in the EU. *Land Use Policy* **2013**, *30*, 446–457. [[CrossRef](#)]
- Benayas, J.M.R.; Martins, A.; Nicolau, J.M.; Schulz, J.J. Abandonment of agricultural land: An overview of drivers and consequences. *CABI Rev.* **2007**, *2*, 14. [[CrossRef](#)]
- Kitano, S. Estimation of determinants of farmland abandonment and its data problems. *Land* **2021**, *10*, 596. [[CrossRef](#)]
- Xu, D.; Deng, X.; Guo, S.; Liu, S. Labor migration and farmland abandonment in rural China: Empirical results and policy implications. *J. Environ. Manag.* **2019**, *232*, 738–750. [[CrossRef](#)]

14. Lasanta, T.; Arnáez, J.; Pascual, N.; Ruiz-Flaño, P.; Errea, M.P.; Lana-Renault, N. Space–time process and drivers of land abandonment in Europe. *Catena* **2017**, *149*, 810–823. [[CrossRef](#)]
15. Statuto, D.; Cillis, G.; Picuno, P. Using Historical Maps within a GIS to Analyze Two Centuries of Rural Landscape Changes in Southern Italy. *Land* **2017**, *6*, 65. [[CrossRef](#)]
16. Estel, S.; Kuemmerle, T.; Alcántara, C.; Levers, C.; Prishchepov, A.; Hostert, P. Mapping farmland abandonment and recultivation across Europe using MODIS NDVI time series. *Remote Sens. Environ.* **2015**, *163*, 312–325. [[CrossRef](#)]
17. Santarsiero, V.; Nolè, G.; Lanorte, A.; Tucci, B.; Cillis, G.; Scorza, F.; Murgante, B. A Remote Sensing Methodology to Assess the Abandoned Arable Land Using NDVI Index in Basilicata Region. *Lect. Notes Comput. Sci.* **2021**, *12954*, 695–703. [[CrossRef](#)]
18. Consumo di Suolo, Dinamiche Territoriali e Servizi Ecosistemici Edizione 2021 Rapporto ISPRA SNPA. Available online: <https://www.snpambiente.it/2021/07/14/consumo-di-suolo-dinamiche-territoriali-e-servizi-ecosistemici-edizione-2021/> (accessed on 28 February 2023).
19. Keenleyside, C.; Tucker, G.; McConville, A. *Farmland Abandonment in the EU: An Assessment of Trends and Prospects*; Institute for European Environmental Policy: London, UK, 2010.
20. Cillis, G.; Nolè, G.; Lanorte, A.; Santarsiero, V.; Tucci, B.; Scorza, F.; Murgante, B. Soil Erosion and Land Degradation in Rural Environment: A Preliminary GIS and Remote-Sensed Approach. *Lect. Notes Comput. Sci.* **2021**, *12954*, 682–694. [[CrossRef](#)]
21. Gabellieri, N. La Comunità Europea e il Paesaggio Rurale: Il Caso del Set Aside (1988–1993). 2013. Available online: https://iris.unin.it/retrieve/handle/11572/209682/202501/xx12_Gabellieri_205_ok%281%29.pdf (accessed on 28 February 2023).
22. Lazio, R. Il Consumo di Suolo tra Politiche Ambientali e Politiche Economiche: Un’ Analisi dell’ Impatto dei Programmi di Sviluppo Rurale Nelle Aree Protette della Regione Lazio. 2015. Available online: https://www.researchgate.net/profile/Davide-Marino-2/publication/279183551_Il_consumo_di_suolo_tra_politiche_ambientali_e_politiche_economiche_un\T1\textquoterightanalisi_dell\T1\textquoterightimpatto_dei_Programmi_di_Sviluppo_Rurale_nelle_aree_protette_della_Region_Lazio/links/558d03b608ae591c19da2405/Il-consumo-di-suolo-tra-politiche-ambientali-e-politiche-economiche-unanalisi-dellimpato-dei-Programmi-di-Sviluppo-Rurale-nelle-aree-protette-della-Region-Lazio.pdf (accessed on 28 February 2023).
23. Quaranta, G.; Salvia, R.; Salvati, L.; De Paola, V.; Coluzzi, R.; Imbrenda, V.; Simoniello, T. Long-term impacts of grazing management on land degradation in a rural community of Southern Italy: Depopulation matters. *Land Degrad. Dev.* **2020**, *31*, 2379–2394. [[CrossRef](#)]
24. Munroe, D.K.; van Berkel, D.B.; Verburg, P.H.; Olson, J.L. Alternative trajectories of land abandonment: Causes, consequences and research challenges. *Curr. Opin. Environ. Sustain.* **2013**, *5*, 471–476. [[CrossRef](#)]
25. Blaikie, P.; Brookfield, H. *Land Degradation and Society*. Routledge: Oxfordshire, UK, 2015. [[CrossRef](#)]
26. Pacheco, F.A.L.; Sanches Fernandes, L.F.; Valle Junior, R.F.; Valera, C.A.; Pissarra, T.C.T. Land degradation: Multiple environmental consequences and routes to neutrality. *Curr. Opin. Environ. Sci. Health* **2018**, *5*, 79–86. [[CrossRef](#)]
27. Panagos, P.; Meusburger, K.; Ballabio, C.; Borrelli, P.; Alewell, C. Soil erodibility in Europe: A high-resolution dataset based on LUCAS. *Sci. Total Environ.* **2014**, *479–480*, 189–200. [[CrossRef](#)]
28. Rabia, A.H. Mapping soil erosion risk using RUSLE, GIS and remote sensing techniques. In Proceedings of the 4th International Congress of ECSSS, EUROSOIL, Bari, Italy, 2–6 July 2012; pp. 1–15.
29. Mallick, J.; Alashker, Y.; Mohammad, S.A.-D.; Ahmed, M.; Hasan, M.A. Risk assessment of soil erosion in semi-arid mountainous watershed in Saudi Arabia by RUSLE model coupled with remote sensing and GIS. *Geocarto Int.* **2014**, *29*, 915–940. [[CrossRef](#)]
30. Ganasri, B.P.; Ramesh, H. Assessment of soil erosion by RUSLE model using remote sensing and GIS—A case study of Nethravathi Basin. *Geosci. Front.* **2016**, *7*, 953–961. [[CrossRef](#)]
31. Prasannakumar, V.; Shiny, R.; Geetha, N.; Vijith, H. Spatial prediction of soil erosion risk by remote sensing, GIS and RUSLE approach: A case study of Siruvani river watershed in Attapady valley, Kerala, India. *Environ. Earth Sci.* **2011**, *64*, 965–972. [[CrossRef](#)]
32. Sourn, T.; Pok, S.; Chou, P.; Nut, N.; Theng, D.; Vara Prasad, P.V. Assessment of Land Use and Land Cover Changes on Soil Erosion Using Remote Sensing, GIS and RUSLE Model: A Case Study of Battambang Province, Cambodia. *Sustainability* **2022**, *14*, 4066. [[CrossRef](#)]
33. Stefanidis, S.; Alexandridis, V.; Mallinis, G. A cloud-based mapping approach for assessing spatiotemporal changes in erosion dynamics due to biotic and abiotic disturbances in a Mediterranean Peri-Urban forest. *Catena* **2022**, *218*, 106564. [[CrossRef](#)]
34. Vanmaercke, M.; Poesen, J.; Radoane, M.; Govers, G.; Ocakoglu, F.; Arabkhedri, M. How long should we measure? An exploration of factors controlling the inter-annual variation of catchment sediment yield. *J. Soils Sediments* **2012**, *12*, 603–619. [[CrossRef](#)]
35. Renard, K.G.; Foster, G.R.; Weesies, G.A.; Porter, J.P. RUSLE: Revised universal soil loss equation. *J. Soil Water Conserv.* **1991**, *46*, 30–33.
36. Nolè, G.; Murgante, B.; Calamita, G.; Lanorte, A.; Lasaponara, R. Evaluation of urban sprawl from space using open source technologies. *Ecol. Inform.* **2015**, *26*, 151–161. [[CrossRef](#)]
37. Simoniello, T.; Coluzzi, R.; D’Emilio, M.; Imbrenda, V.; Salvati, L.; Sinisi, R.; Summa, V. Going Conservative or Conventional? Investigating Farm Management Strategies in between Economic and Environmental Sustainability in Southern Italy. *Agronomy* **2022**, *12*, 597. [[CrossRef](#)]
38. Tucci, B.; Nolè, G.; Lanorte, A.; Santarsiero, V.; Cillis, G.; Scorza, F.; Murgante, B. Assessment and Monitoring of Soil Erosion Risk and Land Degradation in Arable Land Combining Remote Sensing Methodologies and RUSLE Factors. *Lect. Notes Comput. Sci.* **2021**, *12954*, 704–716. [[CrossRef](#)]

39. Santarsiero, V.; Lanorte, A.; Nolè, G.; Cillis, G.; Murgante, B. Land Use Change Evaluation in an Open-Source GIS Environment: A Case Study of the Basilicata Region (Southern Italy). In *Computational Science and Its Applications—ICCSA 2022: 22nd International Conference, Malaga, Spain, 4–7 July 2022, Proceedings, Part II*; Springer International Publishing: Cham, Switzerland, 2022; Volume 13376, ISBN 9783031104497.
40. Samela, C.; Imbrenda, V.; Coluzzi, R.; Pace, L.; Simoniello, T.; Lanfredi, M. Multi-Decadal Assessment of Soil Loss in a Mediterranean Region Characterized by Contrasting Local Climates. *Land* **2022**, *11*, 1010. [[CrossRef](#)]
41. Imbrenda, V.; Quaranta, G.; Salvia, R.; Egidi, G.; Salvati, L.; Prokopovà, M.; Coluzzi, R.; Lanfredi, M. Land degradation and metropolitan expansion in a peri-urban environment. *Geomat. Nat. Hazards Risk* **2021**, *12*, 1797–1818. [[CrossRef](#)]
42. Belay, T.; Mengistu, D.A. Land use and land cover dynamics and drivers in the Muga watershed, Upper Blue Nile basin, Ethiopia. *Remote Sens. Appl. Soc. Environ.* **2019**, *15*, 100249. [[CrossRef](#)]
43. Bocco, G.; Mendoza, M.; Velázquez, A. Remote sensing and GIS-based regional geomorphological mapping—A tool for land use planning in developing countries. *Geomorphology* **2001**, *39*, 211–219. [[CrossRef](#)]
44. Coluzzi, R.; Bianchini, L.; Egidi, G.; Cudlin, P.; Imbrenda, V.; Salvati, L.; Lanfredi, M. Density matters? Settlement expansion and land degradation in Peri-urban and rural districts of Italy. *Environ. Impact Assess. Rev.* **2022**, *92*, 106703. [[CrossRef](#)]
45. Santarsiero, V.; Nolè, G.; Lanorte, A.; Tucci, B.; Cillis, G.; Murgante, B. Remote Sensing and Spatial Analysis for Land-Take Assessment in Basilicata Region (Southern Italy). *Remote Sens.* **2022**, *14*, 1692. [[CrossRef](#)]
46. Santarsiero, V.; Nolè, G.; Lanorte, A.; Tucci, B.; Baldantoni, P.; Murgante, B. Evolution of Soil Consumption in the Municipality of Melfi (Southern Italy) in Relation to Renewable Energy. *Lect. Notes Comput. Sci.* **2019**, *11621*, 675–682. [[CrossRef](#)]
47. Alcantara, C.; Kuemmerle, T.; Prishchepov, A.V.; Radeloff, V.C. Mapping abandoned agriculture with multi-temporal MODIS satellite data. *Remote Sens. Environ.* **2012**, *124*, 334–347. [[CrossRef](#)]
48. Joshi, N.; Baumann, M.; Ehammer, A.; Fensholt, R.; Grogan, K.; Hostert, P.; Jepsen, M.R.; Kuemmerle, T.; Meyfroidt, P.; Mitchard, E.T.A.; et al. A Review of the Application of Optical and Radar Remote Sensing Data Fusion to Land Use Mapping and Monitoring. *Remote Sens.* **2016**, *8*, 70. [[CrossRef](#)]
49. Di Palma, F.; Amato, F.; Nolè, G.; Martellozzo, F.; Murgante, B. A SMAP Supervised Classification of Landsat Images for Urban Sprawl Evaluation. *ISPRS Int. J. Geo-Inf.* **2016**, *5*, 109. [[CrossRef](#)]
50. Duarte, L.; Cunha, M.; Teodoro, A.C. Comparing hydric erosion soil loss models in rainy mountainous and dry flat regions in Portugal. *Land* **2021**, *10*, 554. [[CrossRef](#)]
51. Majhi, A.; Shaw, R.; Mallick, K.; Patel, P.P. Towards improved USLE-based soil erosion modelling in India: A review of prevalent pitfalls and implementation of exemplar methods. *Earth-Sci. Rev.* **2021**, *221*, 103786. [[CrossRef](#)]
52. Nolè, G.; Santarsiero, V.; Lanorte, A.; Tucci, B.; Capurso, V.A.; Ronco, F.V.; Murgante, B. Model of Post Fire Erosion Assessment Using RUSLE Method, GIS Tools and ESA Sentinel DATA. *Lect. Notes Comput. Sci.* **2020**, *12253*, 505–516. [[CrossRef](#)]
53. Salvati, L.; Carlucci, M. Estimating land degradation risk for agriculture in Italy using an indirect approach. *Ecol. Econ.* **2010**, *69*, 511–518. [[CrossRef](#)]
54. Costantini, E.A.C.; Urbano, F.; Aramini, G.; Barbetti, R.; Bellino, F.; Bocci, M.; Bonati, G.; Fais, A.; L’Abate, G.; Loj, G. Rationale and methods for compiling an atlas of desertification in Italy. *Land Degrad. Dev.* **2009**, *20*, 261–276. [[CrossRef](#)]
55. Imbrenda, V.; D’Emilio, M.; Lanfredi, M.; Ragosta, M.; Simoniello, T. Indicators of land degradation vulnerability due to anthropic factors: Tools for an efficient planning. In *Sustainable Practices: Concepts, Methodologies, Tools, and Applications*; IGI Global: Hershey, PA, USA, 2014; pp. 1400–1413.
56. Imbrenda, V.; Coluzzi, R.; Lanfredi, M.; Loperte, A.; Satriani, A.; Simoniello, T. Analysis of landscape evolution in a vulnerable coastal area under natural and human pressure. *Geomatics. Nat. Hazards Risk* **2018**, *9*, 1249–1279. [[CrossRef](#)]
57. Satriani, A.; Loperte, A.; Imbrenda, V.; Lapenna, V. Geoelectrical surveys for characterization of the coastal saltwater intrusion in metapontum forest reserve (Southern Italy). *Int. J. Geophys.* **2012**, *2012*, 238478. [[CrossRef](#)]
58. De Santis, F.; Giannossi, M.L.; Medici, L.; Summa, V.; Tateo, F. Impact of physico-chemical soil properties on erosion features in the Aliano area (Southern Italy). *Catena* **2010**, *81*, 172–181. [[CrossRef](#)]
59. Trigila, A.; Iadanza, C.; Guerrieri, L. The IFFI project (Italian landslide inventory): Methodology and results. *Guidel. Mapp. Areas Risk Landslides Eur.* **2007**, *23*, 15–18.
60. Büttner, G.; Feranec, J.; Jaffrain, G.; Mari, L.; Maucha, G.; Soukup, T. The CORINE land cover 2000 project. *EARSeL eProceedings* **2004**, *3*, 331–346.
61. Muscate—Distribution Workshop. Available online: <https://theia.cnes.fr/atdistrib/rocket/#/home> (accessed on 24 January 2023).
62. Carta della Natura—Italiano. Available online: <https://www.isprambiente.gov.it/it/servizi/sistema-carta-della-natura> (accessed on 28 December 2021).
63. Panagos, P.; Jones, A.; Bosco, C.; Kumar, P.S.S. European digital archive on soil maps (EuDASM): Preserving important soil data for public free access. *Int. J. Digit. Earth* **2011**, *4*, 434–443. [[CrossRef](#)]
64. Kim, H.-S.; Julien, P.Y. Soil erosion modeling using RUSLE and GIS on the IMHA Watershed. *Water Eng. Res.* **2006**, *7*, 29–41.
65. Prasannakumar, V.; Vijith, H.; Abinod, S.; Geetha, N. Estimation of soil erosion risk within a small mountainous sub-watershed in Kerala, India, using Revised Universal Soil Loss Equation (RUSLE) and geo-information technology. *Geosci. Front.* **2012**, *3*, 209–215. [[CrossRef](#)]

66. Wischmeier, W.H.; Smith, D.D. *Predicting Rainfall Erosion Losses: A Guide to Conservation Planning*; Department of Agriculture, Science and Education Administration: Hyattsville, MD, USA, 1978.
67. CFD Basilicata. Available online: <http://www.centrofunzionalebasilicata.it/it/> (accessed on 24 January 2023).
68. Capolongo, D.; Pennetta, L.; Piccarreta, M.; Fallacara, G.; Boenzi, F. Spatial and temporal variations in soil erosion and deposition due to land-levelling in a semi-arid area of Basilicata (Southern Italy). *Earth Surf. Processes Landf. J. Br. Geomorphol. Res. Group* **2008**, *33*, 364–379. [[CrossRef](#)]
69. Terranova, O.; Antronico, L.; Coscarelli, R.; Iaquina, P. Soil erosion risk scenarios in the Mediterranean environment using RUSLE and GIS: An application model for Calabria (southern Italy). *Geomorphology* **2009**, *112*, 228–245. [[CrossRef](#)]
70. Bircher, P.; Liniger, H.P.; Prasuhn, V. Comparing different multiple flow algorithms to calculate RUSLE factors of slope length (L) and slope steepness (S) in Switzerland. *Geomorphology* **2019**, *346*, 106850. [[CrossRef](#)]
71. Farhan, Y.; Nawaiseh, S. Spatial assessment of soil erosion risk using RUSLE and GIS techniques. *Environ. Earth Sci.* **2015**, *74*, 4649–4669. [[CrossRef](#)]
72. Moore, I.D.; Wilson, J.P. Length-slope factors for the Revised Universal Soil Loss Equation: Simplified method of estimation. *J. Soil Water Conserv.* **1992**, *47*, 423–428.
73. Kolli, M.K.; Opp, C.; Groll, M. Estimation of soil erosion and sediment yield concentration across the Kolleru Lake catchment using GIS. *Environ. Earth Sci.* **2021**, *80*, 161. [[CrossRef](#)]
74. Samela, C.; Coluzzi, R.; Imbrenda, V.; Manfreda, S.; Lanfredi, M. Satellite flood detection integrating hydrogeomorphic and spectral indices. *GIScience Remote Sens.* **2022**, *59*, 1997–2018. [[CrossRef](#)]
75. Mitsova, H.; Hofierka, J.; Zlocha, M.; Iverson, L.R. Modelling topographic potential for erosion and deposition using GIS. *Int. J. Geogr. Inf. Syst.* **1996**, *10*, 629–641. [[CrossRef](#)]
76. Cencetti, C.; De Rosa, P.; Fredduzzi, A.; Marchesini, I. Erosione dei suoli e grass gis: Esempi di applicazione. In Proceedings of the Geomatics Work, Volume 5—6th Italy GRASS Users Meet, Roma, Italy, 14–15 April 2005; pp. 1–16.
77. Foster, G.R.; Meyer, L.D.; Onstad, C.A. An erosion equation derived from basic erosion principles. *Trans. ASAE* **1977**, *20*, 678–682. [[CrossRef](#)]
78. Zhen, Z.; Chen, S.; Yin, T.; Chavanon, E.; Lauret, N.; Guilleux, J.; Henke, M.; Qin, W.; Cao, L.; Li, J.; et al. Using the Negative Soil Adjustment Factor of Soil Adjusted Vegetation Index (SAVI) to Resist Saturation Effects and Estimate Leaf Area Index (LAI) in Dense Vegetation Areas. *Sensors* **2021**, *21*, 2115. [[CrossRef](#)]
79. Ting Kuo, K.; Sekiyama, A.; Mihara, M. Determining C Factor of Universal Soil Loss Equation (USLE) Based on Remote Sensing. *Int. J. Environ. Rural Dev.* **2016**, *7*, 154–161.
80. De Asis, A.M.; Omasa, K. Estimation of vegetation parameter for modeling soil erosion using linear Spectral Mixture Analysis of Landsat ETM data. *ISPRS J. Photogramm. Remote Sens.* **2007**, *62*, 309–324. [[CrossRef](#)]
81. Lanorte, A.; Cillis, G.; Calamita, G.; Nolè, G.; Pilogallo, A.; Tucci, B.; De Santis, F. Integrated approach of RUSLE, GIS and ESA Sentinel-2 satellite data for post-fire soil erosion assessment in Basilicata region (Southern Italy). *Geomat. Nat. Hazards Risk* **2019**, *10*, 1563–1595. [[CrossRef](#)]
82. Lin, C.Y.; Lin, W.T.; Chou, W.C. Soil erosion prediction and sediment yield estimation: The Taiwan experience. *Soil Tillage Res.* **2002**, *68*, 143–152. [[CrossRef](#)]
83. Van der Knijff, J.M.; Jones, R.J.A.; Montanarella, L. *Soil Erosion Risk: Assessment in Europe*; European Soil Bureau: Brussels, Belgium, 2000.
84. Huete, A.R. A soil-adjusted vegetation index (SAVI). *Remote Sens. Environ.* **1988**, *25*, 295–309. [[CrossRef](#)]
85. Chen, X.; Guo, Z.; Chen, J.; Yang, W.; Yao, Y.; Zhang, C.; Cui, X.; Cao, X. Replacing the red band with the red-SWIR band (0.74pred+0.26pswir) can reduce the sensitivity of vegetation indices to soil background. *Remote Sens.* **2019**, *11*, 851. [[CrossRef](#)]
86. Hu, P.; Sharifi, A.; Tahir, M.N.; Tariq, A.; Zhang, L.; Mumtaz, F.; Shah, S.H.I.A. Evaluation of vegetation indices and phenological metrics using time-series modis data for monitoring vegetation change in Punjab, Pakistan. *Water* **2021**, *13*, 2550. [[CrossRef](#)]
87. Sung, Y.; Lee, G.; Lee, G.; Han, J.; Kim, J.; Lim, K.J.; Kim, K.S. Study on improvement of USLE P factor considering topography and cultivation method. *J. Wetl. Res.* **2019**, *21*, 163–172.
88. Lanorte, A.; Danese, M.; Lasaponara, R.; Murgante, B. Multiscale mapping of burn area and severity using multisensor satellite data and spatial autocorrelation analysis. *Int. J. Appl. Earth Obs. Geoinf.* **2012**, *20*, 42–51. [[CrossRef](#)]
89. Tobler, W.R. A Computer Movie Simulating Urban Growth in the Detroit Region. *Econ. Geogr.* **1970**, *46*, 234–240. [[CrossRef](#)]
90. Peeters, A.; Zude, M.; Käthner, J.; Ünlü, M.; Kanber, R.; Hetzroni, A.; Gebbers, R.; Ben-Gal, A. Getis-Ord's hot- and cold-spot statistics as a basis for multivariate spatial clustering of orchard tree data. *Comput. Electron. Agric.* **2015**, *11*, 140–150. [[CrossRef](#)]
91. Ord, J.K.; Getis, A. Local Spatial Autocorrelation Statistics: Distributional Issues and an Application. *Geogr. Anal.* **1995**, *27*, 286–306. [[CrossRef](#)]
92. Sholagberu, A.T.; Mustafa, M.R.U.; Yusof, K.W.; Hashim, A.M.; Shah, M.M.; Khan, M.W.A.; Isa, M.H. Multivariate logistic regression model for soil erosion susceptibility assessment under static and dynamic causative factors. *Polish J. Environ. Stud.* **2019**, *28*, 3419–3429. [[CrossRef](#)]
93. Lucà, F.; Conforti, M.; Robustelli, G. Comparison of GIS-based gully susceptibility mapping using bivariate and multivariate statistics: Northern Calabria, South Italy. *Geomorphology* **2011**, *134*, 297–308. [[CrossRef](#)]
94. Ayalew, L.; Yamagishi, H. The application of GIS-based logistic regression for landslide susceptibility mapping in the Kakuda-Yahiko Mountains, Central Japan. *Geomorphology* **2005**, *65*, 15–31. [[CrossRef](#)]

95. Tehrany, M.S.; Pradhan, B.; Mansor, S.; Ahmad, N. Flood susceptibility assessment using GIS-based support vector machine model with different kernel types. *Catena* **2015**, *125*, 91–101. [[CrossRef](#)]
96. Kinnell, P.I.A. Raindrop-impact-induced erosion processes and prediction: A review. *Hydrol. Processes* **2005**, *19*, 2815–2844. [[CrossRef](#)]
97. Belief, E. GIS based spatial modeling to mapping and estimation relative risk of different diseases using inverse distance weighting (IDW) interpolation algorithm and evidential belief function (EBF)(Case study: Minor Part of Kirkuk City, Iraq). *Int. J. Eng. Technol.* **2018**, *7*, 185–191.
98. Borrelli, P.; Robinson, D.A.; Fleischer, L.R.; Lugato, E.; Ballabio, C.; Alewell, C.; Meusburger, K.; Modugno, S.; Schütt, B.; Ferro, V.; et al. land use change on soil erosion. *Nat. Commun.* **2012**, *8*, 2013. [[CrossRef](#)] [[PubMed](#)]
99. Cappadonia, C.; Conoscenti, C.; Rotigliano, E. Monitoring of erosion on two calanchi fronts—Northern Sicily (Italy). *Landf. Anal.* **2011**, *17*, 21–25.
100. Piccarreta, M.; Faulkner, H.; Bentivenga, M.; Capolongo, D. The influence of physico-chemical material properties on soil erosion processes in the Badlands of Basilicata, Southern Italy. *Geomorphology* **2006**, *81*, 235–251. [[CrossRef](#)]
101. Da Silva, A.M.; Alvares, C.; Watanabe, C. Natural potential for erosion for Brazilian territory. In *Soil Erosion Studies*; IntechOpen: London, UK, 2011; pp. 3–24.
102. Abdulkadir, T.S.; Muhammad, R.U.M.; Wan Yusof, K.; Ahmad, M.H.; Aremu, S.A.; Gohari, A.; Abdurrasheed, A.S. Quantitative analysis of soil erosion causative factors for susceptibility assessment in a complex watershed. *Cogent Eng.* **2019**, *6*, 1594506. [[CrossRef](#)]
103. Lewis, M. Stepwise versus Hierarchical Regression: Pros and Cons. In Proceedings of the Annual Meeting of the Southwest Educational Research Association, San Antonio, TX, USA, 7 February 2007.
104. Petrocelli, J.V. Hierarchical multiple regression in counseling research: Common problems and possible remedies. *Meas. Eval. Couns. Dev.* **2003**, *36*, 9–22. [[CrossRef](#)]
105. Antonakis, J.; Dietz, J. Looking for validity or testing it? The perils of stepwise regression, extreme-scores analysis, heteroscedasticity, and measurement error. *Personal. Individ. Differ.* **2011**, *50*, 409–415. [[CrossRef](#)]
106. Nandi, A.; Shakoor, A. A GIS-based landslide susceptibility evaluation using bivariate and multivariate statistical analyses. *Eng. Geol.* **2009**, *110*, 11–20. [[CrossRef](#)]
107. Archer, K.J.; Lemeshow, S. Goodness-of-fit test for a logistic regression model fitted using survey sample data. *Stata J.* **2006**, *6*, 97–105. [[CrossRef](#)]
108. Fagerland, M.W.; Hosmer, D.W. A generalized Hosmer–Lemeshow goodness-of-fit test for multinomial logistic regression models. *Stata J.* **2012**, *12*, 447–453. [[CrossRef](#)]
109. Plieninger, T.; Hui, C.; Gaertner, M.; Huntsinger, L. The impact of land abandonment on species richness and abundance in the Mediterranean Basin: A meta-analysis. *PLoS ONE* **2014**, *9*, e98355. [[CrossRef](#)] [[PubMed](#)]
110. Queiroz, C. Managing for Biodiversity and Ecosystem Services in a Context of Farmland Abandonment. Ph.D. Thesis, Stockholm Resilience Centre, Stockholm University, Stockholm, Sweden, 2013.
111. Kust, G.; Andreeva, O.; Cowie, A. Land Degradation Neutrality: Concept development, practical applications and assessment. *J. Environ. Manag.* **2017**, *195*, 16–24. [[CrossRef](#)] [[PubMed](#)]

Disclaimer/Publisher’s Note: The statements, opinions and data contained in all publications are solely those of the individual author(s) and contributor(s) and not of MDPI and/or the editor(s). MDPI and/or the editor(s) disclaim responsibility for any injury to people or property resulting from any ideas, methods, instructions or products referred to in the content.